Project no. GOCE-CT-2003-505539

Project acronym: ENSEMBLES

Project title: ENSEMBLE-based Predictions of Climate Changes and their Impacts

Instrument: Integrated Project

Thematic Priority: Global Change and Ecosystems

D5.30
Evaluation of precipitation extremes in an ensemble of transient regional climate model simulations for the Rhine basin

Due date of deliverable: Month 60 (August 2009)
Actual submission date: Month 60 (August 2009)

Start date of project: 1 September 2004 Duration: 60 Months

Royal Netherland Meteorological Institute

Project co-funded by the European Commission within the Sixth Framework Programme (2002-2006)		
Dissemination Level		
PU	Public	x
PP	Restricted to other programme participants (including the Commission Services)	
RE	Restricted to a group specified by the consortium (including the Commission Services)	
CO	Confidential, only for members of the Consortium (including the Commission Services)	

Martin Hanel, T. Adri Buishand

Evaluation of precipitation extremes in an ensemble of transient regional climate model simulations for the Rhine basin

Royal Netherlands Meteorological Institute (KNMI), Postbus 201, 3730 AE, De Bilt, Netherlands

Submitted to Climate Dynamics

Keywords *Non-stationary index-flood model, GEV distribution, Precipitation extremes, Regional climate change, Rhine basin*

Abstract A non-stationary index-flood model was used to assess the 1-day summer and 5-day winter precipitation maxima in the Rhine basin in an ensemble of 15 transient regional climate model (RCM) simulations. It is assumed that the seasonal precipitation maxima follow a generalized extreme value (GEV) distribution with time varying parameters. The index-flood assumption implies that the dispersion coefficient (the ratio of the scale and the location parameters) and the shape parameter are constant over predefined regions, while the location parameter varies within these regions. A comparison with the estimates from gridded observations shows that these GEV parameters are too large in the summer season, while there is a large overestimation of the location parameter and underestimation of the dispersion coefficient in winter. However, a large part of the biases in the summer season can be ascribed to the low number of stations used for gridding the observations. Though there is considerable variation in the changes of the extreme value distributions among the RCM simulations, common tendencies can be identified. In summer, large quantiles increase as a consequence of an increase of the dispersion coefficient, while there is almost no change of low quantiles. In winter, low quantiles increase because of an increase of the location parameter. This effect is, however, counterbalanced by a decrease of the shape parameter in most RCM simulations, resulting in only a slight increase of large quantiles. Departures from the assumed index-flood model were observed in the Alpine region in the south of the basin (strong spatial heterogeneity in the dispersion coefficient in a number of RCM simulations and a significant altitude dependence of the trend in the location parameter in winter in five RCM simulations).

1 Introduction

Possible changes in precipitation due to the enhanced greenhouse effect may have serious societal impacts. The analyses of theses changes, in particular the changes of precipitation extremes, therefore attract much attention. Studies of precipitation extremes under present and future climate conditions using regional climate models (RCMs) are now rather common (Fowler and Ekström 2009). The projections of changes in the precipitation extremes depend on the RCM, the driving global climate model (GCM) and the emission scenario, and are subject to natural variability. Therefore, an increasing number of studies have considered several RCM simulations to explore the range of potential changes in precipitation extremes. For instance, the ensemble of RCM simulations for Europe from the PRUDENCE project (Christensen and Christensen 2007) has been extensively analyzed. The projections of precipitation changes for individual RCMs were compared (Frei et al. 2006) and attempts were made to combine the multiple RCM outputs to provide multi-model ensemble estimates (Fowler et al. 2007; Fowler and Ekström 2009). Though probability distributions of climate changes from ensembles of climate model simulations have received much attention in recent years, their use could be questioned because of lack of verification for future climate conditions, uncertainties about future greenhouse gas emissions, inter-model dependencies and common biases. A detailed discussion of these difficulties is given by Tebaldi and Knutti (2007).

A large number of RCM simulations has been conducted recently in the framework of the EU funded project ENSEMBLES ("Ensembles-based Predictions of Climate Changes and their Impacts" (Hewitt and Griggs 2004)). In contrast to the PRUDENCE project and

earlier studies, an ensemble of transient high-resolution RCM simulations from the mid 20th century to the mid 21st century was included in this project. Many of these simulations were even continued till the end of the 21st century. Simulations from different GCMs were selected to drive the RCM simulations.

The purpose of this paper is to assess the changes of precipitation extremes in the river Rhine basin (Western Europe) in 15 RCM simulations provided by the ENSEMBLES project and to evaluate their performance with respect to the observed data. Since in this part of Europe short-period convective storms may cause local flooding in summer, whereas multi-day heavy precipitation episodes may have adverse impacts over large areas in winter, we focus on 1-day summer (JJA) and 5-day winter (DJF) precipitation extremes. Hanel et al. (2009) analyzed these extremes in a transient run of the RACMO regional climate model driven by the global ECHAM5 model, one of the ENSEMBLES transient simulations. A non-stationary index-flood model was developed to describe the distribution of the extreme precipitation amounts. The index-flood method is a popular method in hydrology (Hosking and Wallis 1997) which uses spatial pooling of data from several sites in a region to reduce the uncertainty of the estimated quantiles of the extreme value distribution. To deal with extremes in transient RCM simulations an extension of the index-flood model is necessary to allow for changes of distribution parameters over time.

The non-stationary index-flood model is briefly described in Sect. 2. Sect. 3 provides an overview of the Rhine basin, the RCM simulations and the observed data. In Sect. 4 the

estimated distribution parameters in the RCM simulations are compared to those in the observed data for the control period 1961–1990. The projected changes of extreme precipitation for two scenario periods 2031–2050 and 2070–2099 are discussed in Sect. 5. Sect. 6 deals with the adequacy of the fit of the non-stationary index-flood model. The conclusions are presented in Sect. 7.

2 Non-stationary index-flood model

For the assessment of precipitation extremes we use the non-stationary index-flood model of Hanel et al. (2009). This model assumes that the seasonal precipitation maxima follow a generalized extreme value (GEV) distribution, which is defined by its distribution function:

$$F(x) = \exp\left\{-\left[1+\kappa\left(\frac{x-\xi}{\alpha}\right)\right]^{-\frac{1}{\kappa}}\right\}, \qquad \kappa \neq 0,$$

$$F(x) = \exp\left\{-\exp\left[-\left(\frac{x-\xi}{\alpha}\right)\right]\right\}, \qquad \kappa = 0, \tag{1}$$

with ξ, α and κ the location, scale and shape parameter, respectively. The distribution is heavy tailed for positive κ, a negative κ implies a finite upper limit and $\kappa = 0$ results in the Gumbel distribution. The GEV distribution has often been used to model the precipitation maxima from RCM simulations (e.g. Frei et al. 2006; Buonomo et al. 2007; Goubanova and Li 2007; Fowler and Ekström 2009). In the index-flood method, the

dispersion coefficient $\gamma=\alpha/\xi$ is considered. This parameter is comparable with the coefficient of variation.

In the non-stationary index-flood model, the location and scale parameters vary within the region and over the years. The index-flood assumption implies that the precipitation maxima in a certain year are identically distributed within the region after scaling with a site-specific factor. As a consequence, the dispersion coefficient and the shape parameter have to be constant within the region. In Hanel et al. (2009), scaling by the GEV location parameter was considered. The *T*-year quantile (i.e. the value that is exceeded with probability 1/*T*) at any site *s* in year *t* can be then written as

$$Q_T(s,t) = \xi(s,t) q_T(t), \tag{2}$$

where $\xi(s,t)$ is the location parameter at site *s* in year *t* and $q_T(t)$ is a common regional quantile function, given by

$$q_T(t) = 1 - \frac{\gamma(t)}{\kappa(t)}\left\{1 - \left[-\log\left(1-\frac{1}{T}\right)\right]^{-\kappa(t)}\right\}, \qquad \kappa(t) \neq 0,$$

$$q_T(t) = 1 - \gamma(t)\log\left[-\log\left(1-\frac{1}{T}\right)\right], \qquad \kappa(t) = 0, \tag{3}$$

with $\gamma(t)$ and $\kappa(t)$ the time-dependent dispersion coefficient and shape parameter, respectively. The temporal variation of the GEV parameters can be described by the following equations:

$$\xi(s,t) = \xi_0(s)\exp[\xi_1 I(t)], \tag{4}$$

$$\gamma(t) = \exp[\gamma_0 + \gamma_1 I(t)], \tag{5}$$

$$\kappa(t) = \kappa_0 + \kappa_1 I(t). \tag{6}$$

with $I(t)$ a time indicator. Similarly as in Hanel et al. (2009), the seasonal global temperature anomalies of the driving GCM, which are representative of the enhanced greenhouse effect, are used as $I(t)$. To achieve faster convergence of the procedure to estimate the unknown parameters on the right-hand side of Eqs. 4–6, the anomalies are calculated with respect to the whole time series rather than to the control period only. The form of Eq. 4 implies that the relative changes in the quantiles of the distribution are constant over the region and Eq. 5 restricts the dispersion coefficient to positive values.

Other models for the GEV parameters can be considered. The application of Hanel et al. (2009) to the precipitation maxima in the Rhine basin suggests to allow for spatial variation of the dispersion coefficient and to incorporate altitude dependence of the trend in the location parameter. These points are discussed in more detail in Sect. 6.

The parameters $\xi_0(s)$, ξ_1, γ_0, γ_1, κ_0 and κ_1 are estimated by a two-step maximum likelihood procedure. Because the likelihood function in this procedure assumes no temporal and spatial dependence, it can not be used to calculate standard errors of parameter estimates or to construct confidence intervals. Therefore, bootstrap resampling is used for this purpose. Let $X(s,t)$ be the seasonal precipitation maximum at grid box s in year t. The trend is first removed from the $X(s,t)$ values by the transformation

$$\tilde{X}(s,t) = \frac{1}{\hat{\kappa}(t)} \log\left[1 + \frac{\hat{\kappa}(t)}{\hat{\gamma}(t)}\left(\frac{X(s,t)}{\hat{\xi}(s,t)} - 1\right)\right], \tag{7}$$

where the $\widetilde{X}(s,t)$ are the residuals and $\hat{\xi}(s,t)$, $\hat{\gamma}(t)$ and $\hat{\kappa}(t)$ are the maximum likelihood estimates of the GEV parameters $\xi(s, t)$, $\gamma(t)$ and $\kappa(t)$, respectively. Spatial dependence is preserved in the bootstrap samples by resampling the residuals for a certain year simultaneously. The resampled residuals $\widetilde{X}^*(s,t)$ are then transformed back to the original scale using

$$X^*(s,t) = \hat{\xi}(s,t)\left\{1 + \hat{\gamma}(t)\frac{\exp[\hat{\kappa}(t)\widetilde{X}^*(s,t)] - 1}{\hat{\kappa}(t)}\right\} \tag{8}$$

and the parameters $\xi_0(s)$, ξ_1, γ_0, γ_1, κ_0 and κ_1 are re-estimated. For inference on changes in the multi-model ensemble it is also necessary to preserve dependence among the RCM simulations. This can be achieved by using bootstrap samples based on the same sequence of years for all RCMs driven by the same GCM simulation.

The residuals should have a standard Gumbel distribution if the model is correct. This is used to assess the goodness of fit by calculating the Anderson-Darling (A^2) statistic

$$A^2 = N\int_{-\infty}^{\infty}\frac{[F_N(x) - F(x)]^2}{F(x)[1 - F(x)]}dF(x) \tag{9}$$

for each grid box, with N the number of years, $F_N(x)$ the empirical distribution function of the $\widetilde{X}(s,t)$ for the grid box of interest and $F(x)$ the standard Gumbel distribution function, $F(x)=\exp[-\exp(-x)]$. The A^2 statistic provides a powerful test against the departures from the assumed GEV distribution (e.g. Shimokawa and Liao 1999; Laio 2004). Hanel et al. (2009) found that significant values of the A^2 statistic were often accompanied with a relatively low or high value of the dispersion coefficient, suggesting that this statistic is also suitable to asses the index-flood assumption. Global and local

critical values of this statistic were obtained from samples generated from a symmetric multivariate normal distribution. Further details on assessing the uncertainty of parameter estimates and goodness of fit testing can be found in Hanel et al. (2009).

3 Rhine basin and data used

The Rhine is the longest river in Western Europe. It originates in the Swiss Alps and flows into the North Sea in the Netherlands (Fig. 1a). Its basin has an area of 185,000 km^2. Large parts of the basin are situated in Germany (57%) and in Switzerland, France and the Netherlands (together 40%). Mean annual precipitation varies from about 400 mm in the area around Mainz in the centre of the Rhine basin to more than 3000 mm in parts of the Alps. The overall mean annual precipitation is 910 mm.

The index-flood model requires homogeneous regions. In this study, we used the same subdivision of the Rhine basin as Hanel et al. (2009), who distinguished five regions (Fig. 1b) based on the grid box estimates of the GEV dispersion coefficient for the RACMO regional climate model simulation. Region 1 corresponds roughly to the Swiss part of the basin and region 5 to the Dutch part. The homogeneity of regions for all RCM simulations is discussed in Sect. 6.

We analyzed 15 transient RCM simulations driven by seven different runs of five global climate models forced by the SRES A1B emission scenario (Table 1). The three HadCM3 runs result from a perturbed physics ensemble experiment (Murphy et al. 2004; Collins et al. 2006): HadCM3Q0 is a run of the unperturbed model, HadCM3Q3 and HadCM3Q16

are runs of the perturbed model giving the lowest and highest global temperature response to external forcings, respectively. Most of the RCM simulations extend from 1951 to the end of the 21st century (2099 or 2100), being 149 or 150 years long. One simulation begins in 1961, three simulations end in 2050. The RCMs use a common rotated longitude-latitude grid with a horizontal resolution of ≈ 25 km except RegCM_EH5, CNRM_ARP and CRCM_CCC which have different grid geometry but comparable resolution.

For the validation of the precipitation extremes in the RCM simulations we used the E-OBS data set (Haylock et al. 2008), at present available for the period 1950–2006. This data set was derived through interpolation of meteorological station measurements to different grids, including the rotated longitude-latitude grid with a horizontal resolution of ≈ 25 km that is used by the majority of the RCM simulations. The density of stations used to interpolate the data is variable over the Rhine basin and in general much lower than the grid resolution. This implies that only a small fraction of grid boxes contains one or more rainfall stations (Fig. 1b).

Fig. 2a–c shows the basin-average relative bias of the mean seasonal and annual precipitation with respect to the E-OBS for each RCM simulation and Fig. 2d–f gives the regional average bias for each of the five regions of the Rhine basin for the whole RCM ensemble. In summer, the ECHAM5 driven simulations are positively biased, on average by 10–35%. The bias of the HadCM3 driven runs ranges between -20 and 25%, HIR_ARP is negatively biased by more than 50%, whereas the other ARPEGE driven run

(CNRM_ARP) has a slight positive bias of 8%. The bias of the BCM driven runs and CRCM_CCC is 10–25%. In winter, all simulations show a positive bias of 35–80% except CNRM_ARP, CRCM_CCC and the HadCM3Q3 driven runs with biases of 8–27%. The bias in mean winter precipitation is in general stronger in the southern part of the Rhine basin (Fig. 2e). The bias of the mean annual precipitation is 0–50%.

The basin-average relative changes in the mean seasonal and annual precipitation between the periods 1961–1990 and 2070–2099 (1961–1990 and 2021–2050 for CNRM_ARP, HIR_BCM and CRCM_CCC) are given in Fig. 3a–c. The ensemble average changes for each of the five regions are depicted in Fig. 3d–f. With the exception of CNRM_ARP, RCA_BCM, HIR_BCM and CRCM_CCC, the RCM simulations show a significant decrease (10–30%) of mean summer precipitation (assessed by Student's t-test at the 0.1 significance level). The mean winter precipitation increases significantly in the ECHAM5 driven simulations (about 20%), RCA_Q3 (12%) and in the simulations driven by BCM (about 15%). The changes are not significant (same t-test) for the rest of the RCM simulations (-10 to 10%). There is a remarkable south-north gradient in the regional average changes of mean winter precipitation in the RCM simulations till the end of the 21st century. The change of mean annual precipitation ranges between -10 and 10%.

In our statistical model, the change of the GEV parameters is related to the change of the seasonal global temperature (anomalies) of the driving GCMs, which are used as the time indicator $I(t)$ in Eqs. 4–6. The average global temperature change over all seven GCMs

between the periods 1961–1990 and 2070–2099 (Table 2) is 2.96°C in summer and 3.21°C in winter. The increase is lower in HadCM3Q3, BCM and CGCM, the largest increase is predicted by HadCM3Q16.

4 Evaluation of simulated precipitation extremes

4.1 Summer

Fig. 4a–c shows boxplots of the basin-average estimates of the GEV parameters for the control period (1961–1990) as derived from 500 bootstrap samples for each RCM simulation and the E-OBS. For each of the regions in Fig. 1b, the estimated values of ξ, γ and κ were obtained from Eqs. 4–6 using the average summer global temperature anomaly of the driving GCM in the control period as $I(t)$. For the E-OBS the anomalies of the HadCRUT3 data set of gridded observed temperatures (Brohan et al. 2006) were used. The estimates of the location parameter for the individual grid boxes were averaged over the region. The basin-average estimates were obtained by averaging the estimates from all five regions. Fig. 4d–f gives for each region the boxplot of the mean parameter estimate for the RCM ensemble and the estimate for the E-OBS. The ensemble mean was for each bootstrap sample obtained by simply averaging the estimates for different RCM simulations.

Compared to the E-OBS, the estimates of the location parameter are 10–30% larger in most of the RCM simulations. Only the estimates for HadRM_Q3, HadRM_Q16 and CNRM_ARP are close to those for the E-OBS, while those for HIR_ARP and CRCM_CCC are 27 and 15% lower, respectively (Fig. 4a). With the exception of region

5, the ensemble average estimates of the location parameter are larger than those from the E-OBS (Fig. 4d). A large part of this difference can be ascribed to the low number of stations used for gridding the E-OBS. In particular, in areas with low station density, stations far outside the grid box significantly contribute to the estimated area-average precipitation over the grid box, resulting in a large amount of spatial smoothing. Hofstra et al. (2009) showed that the upper deciles of the area-averaged daily rainfall amounts in the E-OBS data set tend to be too low, especially in the Alpine area. The difference in the estimated location parameters is relatively small in region 5 where more stations were available for gridding than in the other regions. The bias in the location parameter is strongly related to the bias in the standard deviation of the 1-day precipitation amounts (Fig. 5a), which is mainly due to the simulation of relatively many high values.

The estimates of the dispersion coefficient (Fig. 4b) in the RCM simulations are 20–50% larger than those for the E-OBS, except for the ECHAM5 driven models, RCA_Q3 and CRCM_CCC, for which the difference is -15–15%. The ensemble mean of the estimated dispersion coefficient exceeds the estimate for the E-OBS data by about 20% for all regions in the Rhine basin except for region 2, where the boxplot for the ensemble mean overlaps with that for the E-OBS (Fig. 4e). In the case of a positive bias in the location parameter as observed for most RCM simulations in Fig. 4a, the positive bias of the dispersion coefficient implies that the relative bias in the scale parameter is larger than that in the location parameter. The scale parameter is strongly related to the mean excess of the daily values Y exceeding a high threshold u, i.e, $E(Y - u | Y > u)$. The mean excess is proportional to the scale parameter of the generalized Pareto distribution in the

underlying peaks-over-threshold model (e.g. Coles 2001). For the Gumbel distribution (κ = 0), the mean excess provides an alternative estimate of α. The threshold u should be (nearly) as high as the value of the location parameter. The 99th percentile can be taken in the case of seasonal maxima of daily precipitation. Fig. 5b shows that the bias in the mean excess over this threshold largely explains the bias in the GEV scale parameter α. Note further from Fig. 5 that the relative bias in $\hat{\alpha}$ is more than twice as large as that in $\hat{\xi}$. This may partly be due to a larger amount of smoothing of the E-OBS data in more extreme situations.

The shape parameter is positive (Fréchet distribution) in the RCM simulations and in the E-OBS, however, almost all RCMs show a slight overestimation of this parameter (Fig. 4c). Nevertheless, the estimate for the RCM simulations is close to the value of 0.15 that was proposed by Koutsoyiannis (2004) as a geographically constant shape parameter of the distribution of 1-day annual maximum precipitation, based on an analysis of point rainfall data in Europe and North America. The 1-day annual maxima often occur in the summer season.

4.2 Winter

Fig. 6 gives the estimates of the GEV parameters for the control period for the winter season. The basin-average estimates of the location parameter are positively biased by 10–50% with respect to the E-OBS (Fig. 6a). Only CRCM_CCC underestimates this parameter by 9%, the average bias is 28%. In region 1, the average bias is about 45% (Fig. 6d), however, some of the RCM simulations (REMO_EH5, HIR_ARP) are biased

by more than 70% in this region (not shown). The average bias in the rest of the basin is 22%. Because 5-day winter precipitation exhibits a much stronger spatial correlation than 1-day summer precipitation, the 5-day winter extremes in the E-OBS suffer much less from spatial smoothing due to the gridding procedure. However, winter precipitation is more liable to undercatch, in particular snowfall. The E-OBS data were not corrected for this. Frei et al. (2003) give an estimate of 11% of the average undercatch in the Alpine area for the winter season. Due to a smaller fraction of snowfall, the undercatch is expected to be lower in the rest of the basin and thus can only explain part of the 46% bias in the simulated mean precipitation. In addition, the RCMs overestimate the standard deviation of the 5-day precipitation by 20% (not shown). Since this overestimation is smaller than the bias in the mean, the coefficient of variation is underestimated (17%). This partly accounts for the underestimation of the dispersion coefficient (22%) which is found in all RCM simulations (Fig. 6b). Only for the runs driven by HadCM3Q3 the bias in the dispersion coefficient is not much more than 10%. There is a clear south-north gradient in the estimates of the dispersion coefficient both in the simulations and in the E-OBS (Fig. 6e). While the shape parameter is negative (reverse Weibull distribution) in the E-OBS, it is close to zero (Gumbel distribution) in the RCMs (Fig. 6c).

5 Projected changes of precipitation extremes

5.1 Summer

Fig. 7 shows the basin-average of the estimated changes in the GEV parameters $\xi(t)$, $\gamma(t)$,and $\kappa(t)$ between the control period (1961–1990) and the two scenario periods (2031–2050 and 2071–2099) for the 1-day summer precipitation extremes. The change is a

relative change (for $\xi(t)$ and $\gamma(t)$) or an absolute change (for $\kappa(t)$) of the average estimates in the corresponding periods. To obtain the changes for the first scenario period only the data to 2050 were used for fitting the statistical model also in the case of the simulations ending at the end of the 21st century. The differences between RCM simulations are in general not large compared to their uncertainty as indicated by the boxes in Fig. 7a–f. On average, there is no change in the location parameter. The dispersion coefficient increases by about 21% at the end of the 21st century, and the shape parameter increases slightly (on average by 0.025). A notable point is the relatively large increase in the dispersion coefficient (≈ 30%) in the RCA_Q16 simulation for the second scenario period, in contrast with a slight decrease in this parameter for the first scenario period. This suggests that the log-linear relationship in Eq. 5 for the trend in the dispersion coefficient may not be adequate for this simulation. The ensemble mean changes in the location parameter (Fig. 7g) are slightly negative (between -3 and -1%) in regions 1, 3, 4 and 5 and positive (4 %) in region 2. This might be a consequence of weaker summer drying in region 2 predicted by a number of simulations (cf. Fig. 3d), which was already discussed for the RACMO_EH5 simulation by Hanel et al. (2009).

Fig. 8 gives the basin-average relative changes of various quantiles between the control period and the two scenario periods. The thin lines represent the basin-average change for the individual RCM simulations, the thick line corresponds to the ensemble mean. For a number of return periods, the minimal and maximal relative basin-average change in the RCM ensemble was found for each of the 500 bootstrap samples used to estimate the

uncertainty of the changes in the GEV parameters in Fig. 7. The envelopes in Fig. 8 correspond to the 5th percentiles of these minima and 95th percentiles of these maxima.

The change in the 2-year quantile is strongly related to the change in the location parameter, therefore, there is on average little change in this quantile. However, as a consequence of the increase of the dispersion coefficient, larger quantiles increase. The average increase of the 50-year quantile is 12 and 18% for the two scenario periods, respectively. All RCM simulations show this behaviour in the scenario period 2070–2099, except RCA_Q3, in which the relative change decreases at long return periods due to a decrease in the shape parameter (Fig. 7c). The increase in large quantiles is in contrast to the decrease in the mean precipitation (Fig. 3a), which is in agreement with previous studies of Christensen and Christensen (2004) and Frei et al. (2006) based on the PRUDENCE project data. The uncertainty of the relative changes as indicated by the shaded area in Fig. 8 is roughly the same in both scenario periods: 40 and 70% for the change of the 2- and 50-year quantile, respectively. The rather large uncertainty of the changes in the 50-year quantile is partly due to natural variability in the occurrence of large daily rainfall events in summer.

5.2 Winter

The estimated changes in the GEV parameters for the 5-day winter precipitation extremes are given in Fig. 9. The location parameter increases in most RCM simulations (on average by 13% at the end of 21st century). The ECHAM5 driven simulations in the first scenario period and the ARPEGE driven simulations in both scenario periods, however,

show almost no change in this parameter. The change in the location parameter is larger in the north of the basin: the ensemble mean increase for the second scenario period is 6% in region 1 and 19% in region 5 (Fig. 9g). The change in the dispersion coefficient in the first scenario period does not show a clear picture: the estimated change ranges from -20 to 20%. In the second scenario period, the dispersion coefficient stays more or less constant in most of the simulations, only RCA_BCM and the RCM simulations driven by HadCM3Q3 predict a decrease and HIR_ARP an increase in this parameter. The average change in this parameter is small (3 and -3% for the two scenario periods, respectively). Most models show a decrease of the shape parameter in the second scenario period. The average decrease is 0.06 at the end of the 21st century, however, for RACMO_EH5, RCA_EH5 and RCA_BCM the decrease is about twice as large.

The contrast between the estimated changes in the GEV parameters for the two scenario periods for the ECHAM5 driven simulations is remarkable. Surprisingly, it turned out that the choice of the time indicator $I(t)$ in Eqs. 4–6 strongly influences the estimated changes for the first scenario period. The positive trends in the dispersion coefficient and shape parameter were not found in the ECHAM5 driven simulations if their winter temperature anomalies for the Rhine basin were considered as time indicator instead of global temperature anomalies. The choice of a different time indicator has little effect on the estimated changes for the second scenario period as was already found by Hanel et al. (2009) for the RACMO_EH5 simulation.

Fig. 10 depicts the basin-average relative changes of the quantiles for the winter season. The substantial average increase in the location parameter leads to an increase of the low quantiles. In the first scenario period, the majority of the RCM simulations show in addition a decrease either in the dispersion coefficient or in the shape parameter which counterbalances the increase in the location parameter and leads to a decrease of the relative change of the quantiles with increasing return period. This is not the case for the ECHAM5 driven simulations and HIR_ARP in which the location parameter stays almost constant but the dispersion coefficient, and in three of these simulations (RACMO_EH5, REMO_EH5 and RCA_EH5) also the shape parameter, increases (Fig. 9a–c). As a result, the 50-year quantiles increase and there is little change of the 2-year quantiles for these simulations. The ensemble mean relative change in the quantiles is nearly constant (6%) for return periods between 2 and 50 years in the first scenario period. In the second scenario period, the increase at short return periods caused by the increase in the location parameter is counterbalanced by the decrease in the shape parameter leading to smaller changes as the return period gets longer. Only HadRM_Q16 and HIR_ARP show a larger increase at long return periods than at short return periods due to the increase in the dispersion coefficient and absence of the negative trend in the shape parameter. The ensemble mean change of the 2-year quantile is 13%, while the change in the 50-year quantile is relatively small (6%). This slight change in large quantiles is distinct from the clear increase in mean winter precipitation (Fig. 3b), which is typical for the majority of the considered RCM simulations. The uncertainty is significantly lower than in summer, however, still large: the width of the area between the envelopes is 30% at the 2-year return period for both scenario periods and 70% and 50% at the 50-year return period for

the two scenario periods, respectively. The large range for the change in the 50-year quantile for the first scenario period is partly due to the dubious changes in the GEV parameters in the ECHAM5 driven simulations.

6 Validation of the statistical model

For both seasons, the A^2 statistic was calculated for each grid box and each RCM simulation. Hanel et al. (2009) considered both a local goodness of fit test for each grid box separately and a global test for all grid boxes in a region simultaneously. It is often difficult to draw conclusions from the results of local tests because of spatial dependence. Clusters of grid boxes may then fail the Anderson-Darling test even if the model provides an adequate fit. In a global test, the null hypothesis of an adequate fit is rejected if the A^2 statistic exceeds a critical value at one or more grid boxes in the region. The determination of the global critical values requires a large number of bootstrap samples for each region, season and RCM simulation. In order to save computer time, we determined the 0.1 global critical values for a subset of models and regions for both seasons to explore their typical range. In summer, these critical values were between 1.80 and 2.36, and in winter between 1.65 and 2.00. A systematic difference between the critical values of the shorter and longer simulations was not found. A value slightly exceeding the upper limit of the range of the calculated global critical values (2.45 for summer and 2.10 for winter) was taken as the critical threshold of the A^2 statistic for all regions and RCM simulations. The rejection rate is thus somewhat lower than that of a global test at the 0.1 global significance level.

Table 3 gives the percentages of rejected grid boxes for region 1 and regions 2–5 for both seasons and all RCM simulations. Though the percentage of rejected grid boxes is of some concern for a number of RCM simulations for regions 2–5 (7% in summer for RCA_Q16 and 8% in winter for CLM_Q0, RCA_BCM and HIR_BCM), it is really problematic for region 1. This is not surprising because of the complex orography in the Alpine area. For some RCM simulations more than 30% of the grid boxes are rejected in summer or winter making the results of these simulations very questionable. The lack of fit is largely related to heterogeneity of the dispersion coefficient as is clear from Fig. 11. The upper panel (Fig. 11a) shows the histograms and spatial distribution of the estimates of γ_0, which were obtained by fitting the stationary model (i.e. with $I(t)=0$ in Eqs. 4–6) to the 5-day winter maxima for the period 1961–1990 at each grid box in region 1 for the E-OBS, RACMO_EH5, RCA_Q3 and HIR_BCM. The lower panel (Fig. 11b) gives the spatial distribution of the A^2 values for the non-stationary index-flood model. The grid boxes with large A^2 values match quite well the grid boxes with a relatively small or large γ_0. Therefore, as suggested by Hanel et al. (2009), we fitted an alternative model allowing the dispersion coefficient to vary over the region, simply by modifying Eq. 5 to $\gamma(s,t)=\exp[\gamma_0(s)+\gamma_1 I(t)]$. To evaluate the performance of this statistical model, the 0.1 global critical values for a subset of simulations and regions were calculated for both seasons. The critical values were in the interval 1.20–1.52 in summer and 1.12–1.45 in winter leading to critical thresholds of 1.55 and 1.50 for summer and winter, respectively. The percentages of rejected grid boxes (Table 4) for the alternative non-stationary GEV model are much lower than those for the index-flood model.

A consequence of heterogeneity of the dispersion coefficient is that the relative changes in the quantiles are no longer constant over the region. To justify the summary Figs. 8 and 10, we compared the relative changes in quantiles obtained by the index-flood model with the regional-average relative changes in quantiles from the alternative model for region 1 for all RCM simulations. These differences were in both seasons less than 5% for all simulations (not shown). The comparison for the RCA_Q3 simulation for the winter season is given in Fig. 12a. The dashed lines represent the average relative changes of the quantiles for the subset of grid boxes with $\hat{\gamma}_0(s) < Q_{0.33}(\hat{\gamma}_0)$ and $\hat{\gamma}_0(s) > Q_{0.66}(\hat{\gamma}_0)$, where $Q_p(\hat{\gamma}_0)$ denotes the *p*-th quantile of the distribution of $\hat{\gamma}_0$ in region 1. It can be seen that there is almost no difference between the changes in the quantiles for grid boxes with large and small values of $\hat{\gamma}_0$. The regional-average difference between the two statistical models is less than 2% for all quantiles. Fig. 12b gives the ensemble mean relative change in region 1 for both statistical models together with envelopes. The difference in the ensemble mean is negligible, however, the uncertainty of the changes in quantiles is slightly larger for the alternative model with spatially varying γ_0.

Giorgi et al. (1997) studied the altitude dependence of the changes in seasonal mean temperature and precipitation in an RCM simulation. The relative increase in mean winter precipitation turned out to be smaller at high altitudes (though the absolute increase was larger). Hanel et al. (2009) found that the same applies for the trend ξ_1 in the location parameter of the 5-day winter precipitation maxima in the RACMO_EH5 simulation. To assess the significance of this altitude dependence we considered a non-

stationary index-flood model allowing for two different values of the trend in the location parameter: $\xi_{1<800}$ for grid boxes below 800 m and $\xi_{1>800}$ for grid boxes above 800 m. This model was fitted to the 5-day winter precipitation maxima in region 1 in each RCM simulation. The statistical significance of the observed differences d_{800} between the estimates of $\xi_{1<800}$ and $\xi_{1>800}$ was evaluated by a simple bootstrap test. The test compares d_{800} with the estimated differences from 500 bootstrap samples in which the altitude dependence is removed in the same way as in the bootstrap test in Appendix A of Hanel et al. (2009). Table 5 gives d_{800} and the *p*-values of the test. The difference d_{800} is positive for all RCM simulations and statistically significant at the 0.1 level for five RCM simulations (RACMO_EH5, REMO_EH5, HadRM_Q0, RCA_Q16 and RCA_BCM). The physical cause of the altitude dependence of the changes in the location parameter is not clear. There is, e.g., a large difference between the RACMO_EH5 and REMO_EH5 simulations and the other two simulations (RCA_EH5 and RegCM_EH5) driven by the ECHAM5 global model. The changes in the large-scale circulation are similar in these four RCM simulations, also if only days on which the 99th percentile of the precipitation amount is exceeded are considered. Though there is little evidence of an altitude dependent change of ξ in the RCA_EH5 and RCA_Q3 simulations, this altitude dependence is statistically significant in the RCA_Q16 and RCA_BCM simulations. Fig. 13a displays the estimates of ξ_1 for all grid boxes for the 5-day precipitation maxima in the HadRM_Q0 simulation versus altitude together with the estimates of $\xi_{1<800}$ and $\xi_{1>800}$ for region 1. The grid box estimates of ξ_1 were obtained by fitting the non-stationary GEV model to the precipitation maxima at each grid box. Fig. 13b compares the relative changes in the quantiles from the model with constant trend in the location parameter

with those for the model with two values of the trend in this parameter for the same simulation for region 1. In the altitude-dependent model for this simulation, all quantiles show an increase at the grid boxes below 800 m and a decrease at the grid boxes above 800 m. However, the ensemble mean relative changes of the quantiles for the altitude-dependent model (not shown) are almost identical to those for the model with constant ξ_1.

7 Conclusions

The non-stationary index-flood model of Hanel et al. (2009) was applied to 15 RCM simulations conducted in the framework of the ENSEMBLES project in order to explore the impact of the enhanced greenhouse effect on the 1-day summer and 5-day winter precipitation extremes in the Rhine basin. The maxima from the grid boxes were pooled over predefined regions to reduce the uncertainty of the changes in the quantiles of the precipitation extremes. Five regions were discriminated. The changes of various quantiles of precipitation extremes can be well understood by looking at the changes of the parameters of the underlying GEV distribution.

The performance of the RCM simulations was checked by comparing the estimates of the GEV parameters with those obtained for the E-OBS data set for the control period (1961–1990). The location parameter of the 1-day summer maxima for the RCM simulations is on average larger than that for the E-OBS. However, a large part of this difference is most likely due to the reduction of the 1-day summer maxima in the E-OBS caused by the low density of stations used for gridding the observations. The dispersion coefficient is larger and the shape parameter slightly larger in most RCM simulations than in the E-

OBS in the summer season. In the winter season, the location parameter is overestimated, especially in region 1. This is strongly related to the overestimation of the mean and standard deviation of 5-day winter precipitation. The overestimation of the mean is about twice as large as that of the standard deviation implying lower relative variability which leads to the underestimation of the dispersion coefficient inherent to all RCM simulations. The shape parameter is larger in the RCM simulations.

Although, there are differences in the estimated changes of the GEV parameters between the RCM simulations, the general behaviour is identical in the majority of the simulations. The change of the distribution of the 1-day summer precipitation extremes results mainly from the increase of the GEV dispersion coefficient. This leads to a relatively large increase of large quantiles, e.g. the 50-year quantile. The RCM ensemble average increase of this quantile is 12 and 18% for the two scenario periods (2031–2050 and 2070–2099), respectively, and there is little change in the 2-year quantile. The lower quantiles of the distribution of the 5-day winter precipitation maxima generally increase due to an increase of the GEV location parameter, which is related to the increase of mean winter precipitation. The average increase of the 2-year quantile is 6% for the first scenario period and 13% for the second scenario period. For the 50-year quantile this increase is counterbalanced by the decrease of the GEV shape parameter at the end of the 21st century in the majority of the RCM simulations, resulting in a relatively small change of this quantile. The changes of the quantiles in the HadRM_Q16 and HIR_ARP simulations differ considerably from this picture owing to an increase of the dispersion coefficient (enforced by an increase in the shape parameter in HIR_ARP). Moreover, the

decrease in the GEV shape parameters is not clear in the data for the first scenario period 2031–2050. The RCM ensemble average changes in the GEV parameters are in general quite similar in the five regions of the Rhine basin, except for the location parameter in winter, which increases more in the north than in the south of the Rhine basin.

The changes in large quantiles are in both seasons different from the change in the mean. This behaviour is well-known for the summer precipitation maxima. Leander et al. (2008) found little change in large quantiles of the 10-day winter precipitation extremes for the adjacent Meuse basin in an RCM simulation from the PRUDENCE project. This was attributed to a decrease of the coefficient of variation of the 10-day precipitation amounts. For the RCM simulations in this study there is some evidence of a decrease of the coefficient of skewness of the 5-day precipitation amounts rather than a decrease of the coefficient of variation. Further research is needed to get a better understanding of the changes in extreme multi-day precipitation. The non-uniformity of the relative changes of the quantiles of 1- and 5-day precipitation maxima also questions the plausibility of the proportional adjustment of observed data.

Despite the similarities between the estimated changes in GEV parameters in different RCM simulations, the uncertainty about the changes in the quantiles of the extreme value distributions is quite large. The bootstrap estimates of the basin-average relative changes in the 50-year quantile at the end of the 21st century range between 0.88 and 1.57 for the summer season and 0.81 and 1.32 for the winter season. A large part of this uncertainty range is due to the influence of natural variability on these estimates, despite the large

amount of data pooling and averaging of the estimated changes over the five regions to reduce this influence. On the other hand, it is unlikely that the RCM simulations considered in this study cover the whole range of potential changes in the distribution of extreme precipitation amounts. The RCM ensemble was based on only seven GCM simulations. Moreover, three of these referred to the HadCM3 model with different parameter settings and the atmospheric component of BCM has been borrowed from ARPEGE. The study of Lenderink et al. (2007) on generating climate change scenarios for the Netherlands included a number of GCM simulations with an increase in mean summer precipitation of 10 to 20% under the SRES A1B scenario for a similar region as the Rhine basin, which is not found in any RCM simulation analysed in this study.

The assumption of spatial homogeneity of the dispersion coefficient γ is not fulfilled in a number of RCM simulations in region 1. To avoid lack of fit, the non-stationary index-flood model was modified to allow for heterogeneous γ. Although, the fit to the data was improved in this alternative model, the relative change in quantiles of the distribution of precipitation maxima was almost the same as in the model with constant γ. For five RCM simulations the (relative) increase in the location parameter in winter is significantly lower at high altitudes than at low altitudes in region 1. In addition, the same behaviour, though non-significant, was found in the rest of the RCM simulations as well. The physical cause of this altitude dependence is not clear.

The statistical model assumes that the trends in the GEV parameters are approximately (log-)linear in the seasonal global temperature anomalies. Goodness of fit testing in our

RCM ensemble using the A^2 statistic and the analysis of residuals for the RACMO_EH5 simulation by Hanel et al. (2009) did not reject this assumption, even though the changes for the two scenario periods turned out to be considerably different in a number of RCM simulations. This questions the power of the A^2 statistic to detect departures from the (log-)linear model. There is therefore some need for a more specific test. Apart from testing for the significance of a quadratic term in the temperature anomalies, semi-parametric models in which the GEV parameters vary smoothly over time (e.g. Hall and Tajvidi 2000; Ramesh and Davison 2002; Chavez-Demoulin and Davison 2005) could be considered. No parametric form of the trend is imposed in these models. Semi-parametric models are computationally more demanding and need the choice of a smoothing parameter (or smoothing parameters).

Acknowledgements We acknowledge the ENSEMBLES project, funded by the European Commission's 6th Framework Programme through contract GOCE-CT-2003-505539. We thank Albert Klein Tank for comments on a draft of the manuscript.

References

Böhm U, Kücken M, Ahrens W, Block A, Hauffe D, Keuler K, Rockel B, Will A (2006) CLM – the climate version of LM: Brief description and long-term applications. COSMO Newsletter 6:225–235

Brohan P, Kennedy JJ, Harris I, Tett SFB, Jones PD (2006) Uncertainty estimates in regional and global observed temperature changes: A new data set from 1850. J Geophys Res 111: D12106. doi:10.1029/2005JD006548

Buonomo E, Jones R, Huntingford C, Hannaford J (2007) On the robustness of changes in extreme precipitation over Europe from two high resolution climate change simulations. Q J R Meteorol Soc 133:65–81. doi:10.1002/qj.13

Chavez-Demoulin V, Davison AC (2005) Generalized additive models for sample extremes. Applied Statistics 54:207–222

Christensen JH, Christensen OB (2007) A summary of the PRUDENCE model projections of changes in European climate by the end of this century. Clim Dyn 81:7–30. doi: 10.1007/s10584-006-9210-7

Christensen JH, Christensen OB, Lopez P, van Meijgaard E, Botzet M (1996) The HIRHAM4 regional atmospheric climate model. Scientific Report 96–4, DMI, Copenhagen, Denmark

Christensen OB, Christensen JH (2004) Intensification of extreme European summer precipitation in a warmer climate. Global Planet Change 44:107–117. doi:10.1016/j.gloplacha.2004.06.013

Christensen OB, Drews M, Christensen JH, Dethloff K, Ketelsen K, Hebestadt I, Rinke A (2007) The HIRHAM regional climate model version 5 (β). Technical report 06-17, DMI, Copenhagen, Denmark

Coles S (2001) An Introduction to Statistical Modeling of Extreme Values. Springer-Verlag, New York

Collins M, Booth BBB, Harris GR, Murphy JM, Sexton DMH, Webb MJ (2006) Towards quantifying uncertainty in transient climate change. Clim Dyn 27:127–147. doi:10.1007/s00382-006-0121-0

Fowler HJ, Ekström M (2009) Multi-model ensemble estimates of climate change impacts on UK seasonal precipitation extremes. Int J Climatol 29:286–416. doi:10.1002/joc.1827

Fowler HJ, Ekström M, Blenkinsop S, Smith AP (2007) Estimating change in extreme European precipitation using a multimodel ensemble. J Geophys Res 112:D18104. doi:10.1029/2007JD008619

Frei C, Christensen JH, Déqué M, Jacob D, Jones RG, Vidale PL (2003) Daily precipitation statistics in regional climate models: Evaluation and intercomparison for the European Alps. J Geophys Res 108(D3):4124. doi:10.1029/2002JD002287

Frei C, Schöll R, Fukutome S, Schmidli J, Vidale PL (2006) Future change of precipitation extremes in Europe: Intercomparison of scenarios from regional climate models. J Geophys Res 111:D06105. doi:10.1029/2005JD005965

Furevik T, Bentsen M, Drange H, Kindem IKT, Kvamstø NG, Sorteberg A (2003) Description and evaluation of the Bergen climate model: ARPEGE coupled with MICOM. Clim Dyn 21:27–51. doi:10.1007/s00382-003-0317-5

Giorgi F, Hurrell JW, Marinucci MR, Beniston M (1997) Elevation dependency of the surface climate change signal: A model study. J Clim 10:288–296. doi:10.1175/1520-0442(1997)010

Goubanova K, Li L (2007) Extremes in temperature and precipitation around the Mediterranean basin in an ensemble of future climate scenario simulations. Global Planet Change 57:27–42. doi:10.1016/j.gloplacha.2004.06.010

Hall P, Tajvidi N (2000) Nonparametric analysis of temporal trend when fitting parametric models to extreme-value data. Statistical Science 15(2):153–167

Hanel M, Buishand TA, Ferro CAT (2009) A nonstationary index flood model for precipitation extremes in transient regional climate model simulations. J Geophys Res. doi:10.1029/2009JD011712 (in press)

Haylock MR, Hofstra N, Klein Tank AMG, Klok EJ, Jones PD, New M (2008) A European daily high-resolution gridded dataset of surface temperature and precipitation. J Geophys Res 113:D20119. doi:10.1029/2008JD010201

Hewitt CD, Griggs DJ (2004) Ensembles-based predictions of climate changes and their impacts. Eos 85(52):566. doi:10.1029/2004EO520005

Hofstra N, Haylock M, New M, Jones PD (2009) Testing E-OBS European high-resolution gridded dataset of daily precipitation and surface temperature. J Geophys Res (submitted)

Hosking JRM, Wallis JR (1997) Regional frequency analysis. Cambridge University Press

Jacob D (2001) A note to the simulation of the annual and inter-annual variability of the water budget over the Baltic Sea drainage basin. Meteorol Atmos Phys 77(1–4):61–73. doi:10.1007/s007030170017

Jacob D, Andrae U, Elgered G, Fortelius C, Graham LP, Jackson SD, Karstens U, Koepken C, Lindau R, Podzun R, Rockel B, Rubel F, Sass HB, Smith RND, Van den Hurk BJJM, Yang X (2001) A comprehensive model intercomparison study investigating the water budget during the BALTEX-PIDCAP period. Meteorol Atmos Phys 77(1–4):19–43. doi:10.1007/s007030170015

Jones RG, Noguer M, Hassell DC, Hudson D, Wilson SS, Jenkins GJ, Mitchell JFB (2004) Generating high resolution climate change scenarios using PRECIS. Met Office Hadley Centre, Exeter, UK

Jungclaus JH, Keenlyside N, Botzet M, Haak H, Luo J-J, Latif M, Marotzke J, Mikolajewicz U, Roeckner E (2006) Ocean circulation and tropical variability in the coupled model ECHAM5/MPI-OM. J Clim 19:3952–3972. doi:10.1175/JCLI3827.1

Kim S-J, Flato GM, Boer GJ (2003) A coupled climate model simulation of the Last Glacial Maximum, Part 2: approach to equilibrium. Clim Dyn 20:635–661. doi:10.1007/s00382-002-0292-2

Kjellström E, Bärring L, Gollvik S, Hansson U, Jones C, Samuelsson P, Rummukainen M, Ullerstig A, Willén U, Wyser K (2005) A 140-year simulation of European climate with the new version of the Rossby Centre regional atmospheric climate model (RCA3). SMHI Reports Meteorology and Climatology 108, SMHI, Norrköping, Sweden

Koutsoyiannis D (2004) Statistics of extremes and estimation of extreme rainfall: II. Empirical investigation of long rainfall records. Hydrol Sci J 49(4):591–610. doi: 10.1623/hysj.49.4.591.54424.

Laio F (2004) Cramer-von Mises and Anderson-Darling goodness of fit tests for extreme value distributions with unknown parameters. Water Resour Res 40:W09308. doi:10.1029/2004WR003204

Leander R, Buishand TA, van den Hurk BJJM, de Wit MJM (2008) Estimated changes in flood quantiles of the river Meuse from resampling of regional climate model output. J Hydrol 351:331–343. doi:10.1016/j.jhydrol.2007.12.020

Lenderink G, van Ulden A, van den Hurk B, Keller F (2007) A study on combining global and regional climate model results for generating climate scenarios of temperature and precipitation for the Netherlands. Clim Dyn 29:157–176. doi: 10.1007/s00382-007-0227-z

van Meijgaard E, van Ulft LH, van de Berg WJ, Bosveld FC, van den Hurk BJJM, Lenderink G, Siebesma AP (2008) The KNMI regional atmospheric climate model RACMO, version 2.1. Technical Report TR 302, KNMI, De Bilt, The Netherlands

Murphy JM, Sexton DMH, Barnett DN, Jones GS, Webb MJ, Collins M, Stainforth DA (2004) Quantification of modelling uncertainties in a large ensemble of climate change simulations. Nature 430:768–772. doi:10.1038/nature02771

Pal JS, Giorgi F, Bi X, Elguindi N, Solmon F, Gao X, Rauscher SA, Francisco R, Zakey A, Winter J, Ashfaq M, Syed FS, Bell JL, Diffenbaugh NA, Karmacharya J, Konaré A, Martinez D, da Rocha RP, Sloan LC, Steiner AL (2007) Regional climate modelling for the developing world. The ICTP RegCM3 and RegCNET. Bull Amer Meteor Soc 88:1395–1409. doi:10.1175/BAMS-88-9-1395

Plummer D, Caya D, Côté H, Frigon A, Biner S, Giguère M, Paquin D, Harvey R, de Elia R (2006) Climate and climate change over North America as simulated by the Canadian regional climate model. J Clim 19:3112–3132. doi:10.1175/JCLI3769.1

Radu R, Déqué M, Somot S (2008) Spectral nudging in a spectral regional climate model. Tellus 60A: 898–910. doi: 10.1111/j.1600-0870.2008.00341.x

Ramesh NI, Davison AC (2002) Local models for exploratory analysis of hydrological extremes. J Hydrol 256:160–119. doi:10.1016/S0022-1694(01)00522-4

Salas-Mélia D, Chauvin F, Déqué M, Douville H, Gueremy JF, Marquet P, Planton S, Royer JF, Tyteca S (2005) Description and validation of the CNRM-CM3 global coupled model. Available via DIALOG. http://www.cnrm.meteo.fr/scenario2004/paper_cm3.pdf. Accessed 5 Jun 2009

Scinocca JF, McFarlane NA, Lazare M, Li J, Plummer D (2008) Technical Note: The CCCma third generation AGCM and its extension into the middle atmosphere. Atmos Chem Phys 8:7055–7074

Shimokawa T, Liao M (1999) Goodness of fit tests for type-1 extreme-value and 2-parameter Weibull distributions. IEEE Trans Reliab 48(1):79–86

Tebaldi C, Knutti R (2007) The use of the multi-model ensemble in probabilistic climate projections. Phil Trans R Soc A 365:2053–2075. doi:10.1098/rsta.2007.2076

Table 1 Overview of the RCM simulations

acronym	model	period	source	reference
			ECHAM5 driven (Jungclaus 2006)	
RACMO_EH5	RACMO2.1	1950–2100	Royal Netherlands Meteorological Institute (KNMI)	van Meijgaard et al. (2008)
REMO_EH5	REMO5.7	1951–2100	Max Planck Institute for Meteorology (MPI), Germany	Jacob et al. (2001), Jacob (2001)
RCA_EH5	RCA3.0	1951–2100	Swedish Meteorological and Hydrological Institute (SMHI)	Kjellström et al. (2005)
RegCM_EH5	RegCM3	1951–2100	Abdus Salam International Centre for Theoretical Physics (ICTP), Italy	Pal et al. (2007)
			HadCM3Q0, HadCM3Q3, HadCM3Q16 driven (Collins et al. 2006)	
HadRM_Q0	HadRM3.0	1951–2099	Met Office Hadley Centre, UK	Jones et al. (2004)
CLM_Q0	CLM2.4.6	1951–2099	Swiss Federal Institute of Technology Zurich (ETHZ)	Böhm et al. (2006)
HadRM_Q3	HadRM3.0	1951–2099	Met Office Hadley Centre, UK	Jones et al. (2004)
RCA_Q3	RCA3.0	1951–2099	Swedish Meteorological and Hydrological Institute (SMHI)	Kjellström et al. (2005)
HadRM_Q16	HadRM3.0	1951–2099	Met Office Hadley Centre, UK	Jones et al. (2004)
RCA_Q16	RCA3.0	1951–2099	Community Climate Change Consortium for Ireland (C4I)	Kjellström et al. (2005)
			ARPEGE4.5 driven (Salas-Mélia et al. 2005)	
HIR_ARP	HIRHAM5	1951–2100	Danish Meteorological Institute (DMI)	Christensen et al. (2007)
CNRM_ARP	CNRM-RM4.5	1950–2050	National Centre of Meteorological Research (CNRM), France	Radu et al. (2008)
			BCM2.0 driven (Furevik et al. 2003)	
RCA_BCM	RCA3.0	1961–2100	Swedish Meteorological and Hydrological Institute (SMHI)	Kjellström et al. (2005)
HIR_BCM	HIRHAM2	1951–2050	Norwegian Meteorological Institute (METNO)	Christensen et al. (1996)
			CGCM3.1 driven (Kim et al. 2003; Scinocca et al. 2008)	
CRCM_CCC	CRCM4.2.1	1951–2050	Consortium on Regional Climatology and Adaptation to Climate Change (OURANOS), Canada	Plummer et al. (2006)

Table 2 Average global temperature change [°C] in the driving GCMs between the periods 1961–1990 and 2070–2099

GCM	JJA	DJF
ECHAM5	2.81	3.49
HadCM3Q0	3.16	3.45
HadCM3Q3	2.40	2.54
HadCM3Q16	4.09	4.37
ARPEGE	3.19	3.08
BCM	2.45	2.70
CGCM	2.62	2.84
average	2.96	3.21

Table 3 Percentage of grid boxes with an A^2 value larger than the given threshold for the summer (JJA) and winter (DJF) season for the non-stationary index-flood model

	JJA [% $A^2 > 2.45$]		DJF [% $A^2 > 2.10$]	
	region 1	regions 2–5	region 1	regions 2–5
RACMO_EH5	0	2	6	0
REMO_EH5	11	3	20	2
RCA_EH5	2	1	35	2
RegCM_EH5	0	0	13	1
HadRM_Q0	8	2	11	2
CLM_Q0	6	3	30	8
HadRM_Q3	6	0	15	3
RCA_Q3	2	2	39	0
HadRM_Q16	14	2	2	1
RCA_Q16	44	7	14	3
HIR_ARP	18	4	8	4
CNRM_ARP	0	1	11	4
RCA_BCM	20	3	14	6
HIR_BCM	11	4	36	8
CRCM_CCC	3	0	7	0

Table 4 Percentage of grid boxes with an A^2 value larger than the given threshold for the summer (JJA) and winter (DJF) season for the alternative non-stationary GEV model with spatially varying dispersion coefficient

	JJA [% $A^2 > 1.55$]		DJF [% $A^2 > 1.50$]	
	region 1	regions 2–5	region 1	regions 2–5
RACMO_EH5	0	0	0	0
REMO_EH5	2	2	0	0
RCA_EH5	0	0	0	2
RegCM_EH5	0	0	0	0
HadRM_Q0	2	0	2	0
CLM_Q0	0	1	0	0
HadRM_Q3	0	0	3	0
RCA_Q3	0	0	0	0
HadRM_Q16	2	0	0	0
RCA_Q16	2	0	0	0
HIR_ARP	2	0	2	0
CNRM_ARP	0	0	0	0
RCA_BCM	0	0	0	2
HIR_BCM	0	0	0	1
CRCM_CCC	0	0	0	0

Table 5 Differences d_{800} between the estimated trend in the location parameter for the grid boxes below and above 800 m and the *p*-values resulting from the bootstrap test for the winter season (DJF) in region 1

	d_{800}	*p*-value
RACMO_EH5	0.024	0.01
REMO_EH5	0.023	0.02
RCA_EH5	0.003	0.79
RegCM_EH5	0.011	0.34
HadRM_Q0	0.034	0.00
CLM_Q0	0.012	0.25
HadRM_Q3	0.024	0.23
RCA_Q3	0.008	0.63
HadRM_Q16	0.011	0.24
RCA_Q16	0.029	0.00
HIR_ARP	0.009	0.45
CNRM_ARP	0.009	0.61
RCA_BCM	0.022	0.04
HIR_BCM	0.001	0.97
CRCM_CCC	0.008	0.74

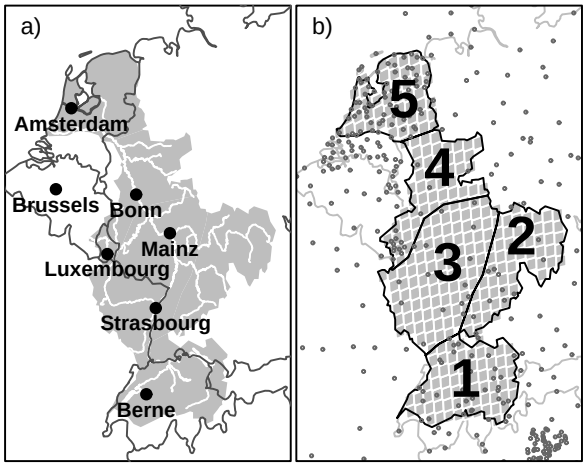

Fig. 1 a The river Rhine basin. **b** Subdivision of the river Rhine basin into five regions. The *rectangles* represent the grid used by the majority of the RCM simulations and by the E-OBS. The *gray dots* show the locations of stations that have been used for gridding the E-OBS data

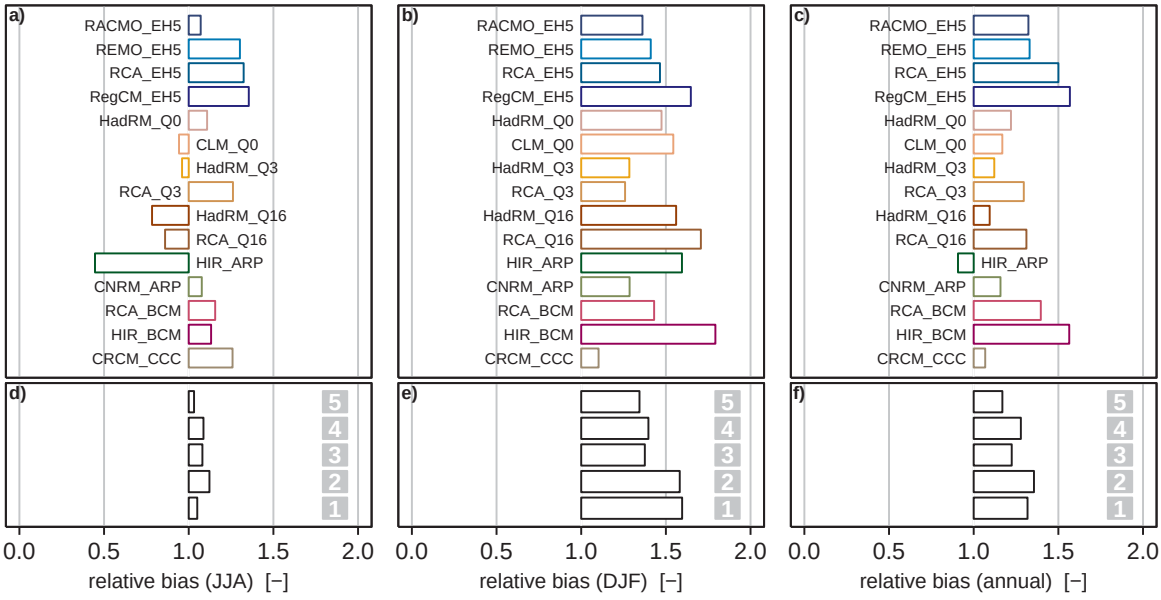

Fig. 2 Relative seasonal and annual bias for the period 1961–1990 of: **a–c** the basin average precipitation for each RCM simulation, and **d–f** the ensemble average precipitation for each of the five regions of the Rhine basin

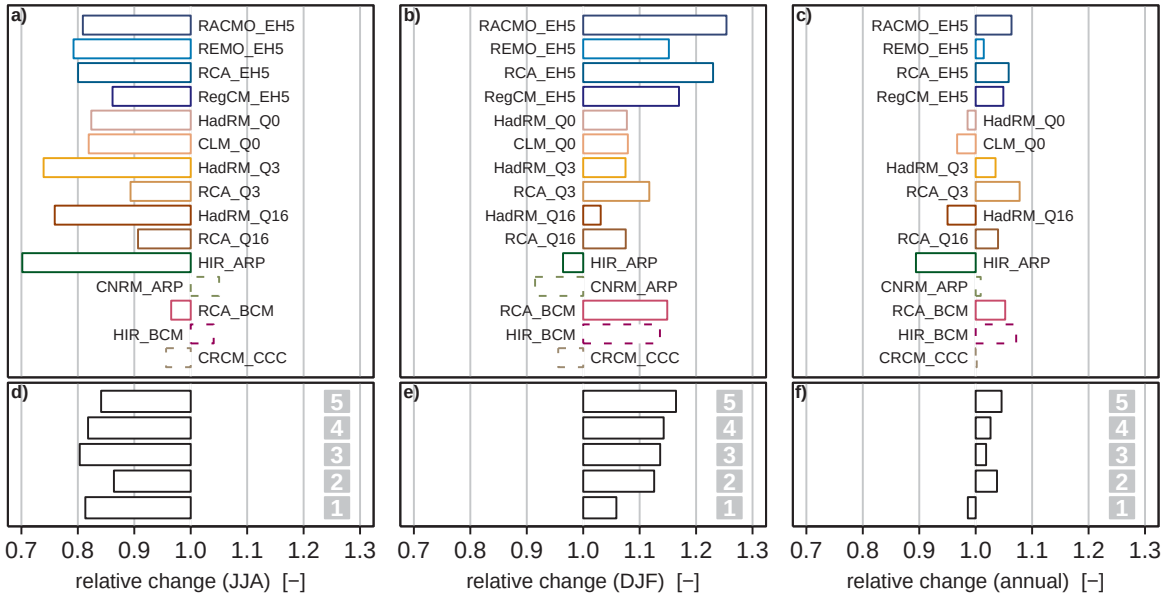

Fig. 3 Relative change of: **a–c** the basin average seasonal and annual precipitation between the periods 1961–1990 and 2031–2050 (*dashed lines*) or 2070–2099 (*solid lines*) for each simulation ending in the middle or at the end of the 21st century, respectively, and **d–f** the average precipitation for each of the five regions of the Rhine basin between the periods 1961–1990 and 2070–2099 for the ensemble of RCM simulations longer than 100 years

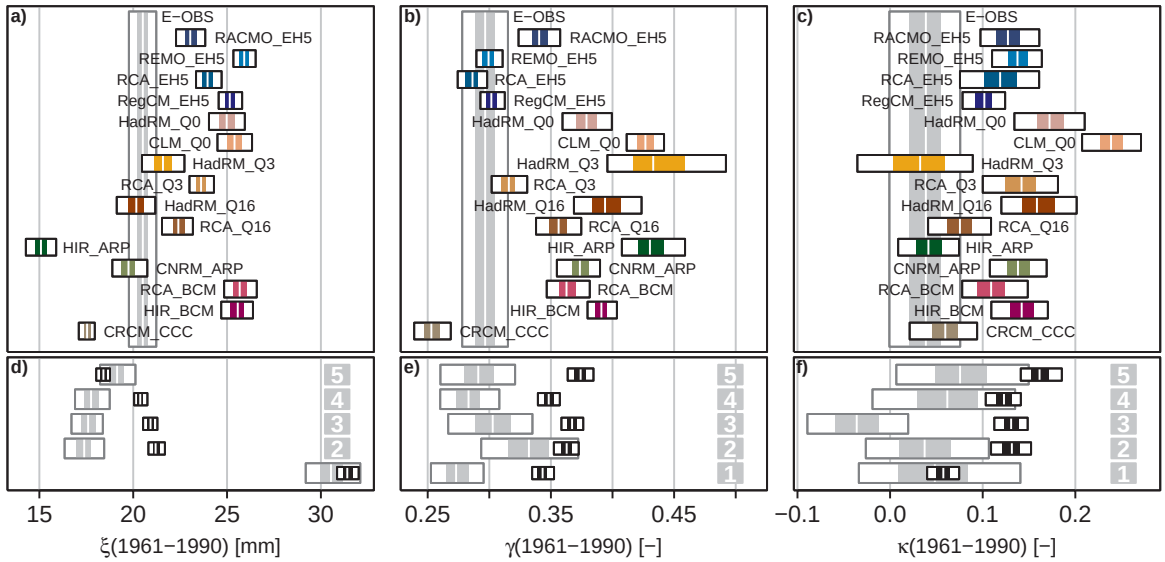

Fig. 4 a–c Basin-average estimates of the GEV parameters for the 1-day summer (JJA) precipitation maxima for all RCMs (*coloured boxes*) and the E-OBS (*large gray box in the background*) for the period 1961–1990, and **d–f** the ensemble average estimates (*black boxes*) of the GEV parameters together with

those for the E-OBS (*gray boxes*) for each of the five regions of the Rhine basin for the period 1961–1990. The boxplots are based on 500 bootstrap samples. The 5th, 25th, 50th, 75th and 95th percentiles of these bootstrap samples are indicated

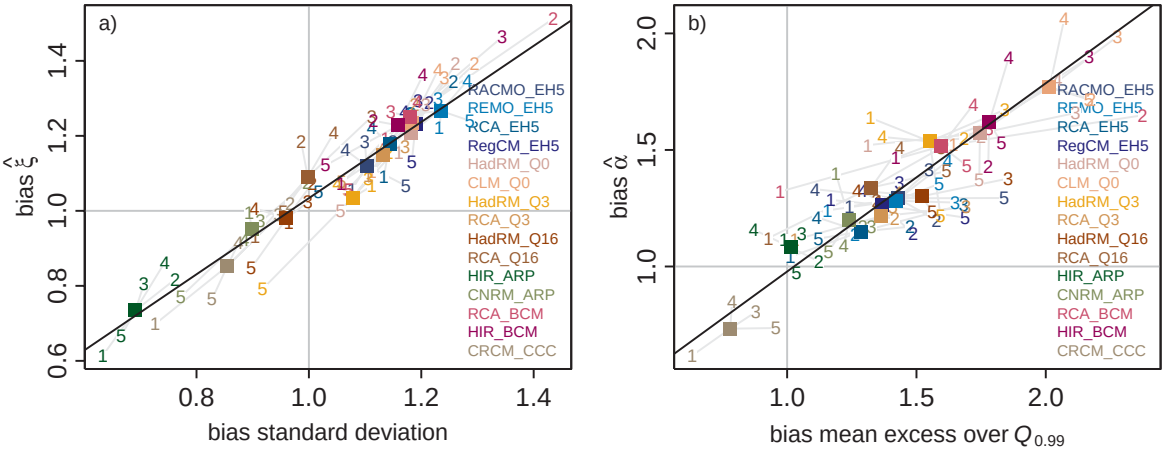

Fig. 5 Bias in the estimated GEV parameters for the 1-day summer (JJA) precipitation extremes: **a** relative bias in the location parameter $\hat{\xi}$ versus the relative bias in the standard deviation, and **b** relative bias in the scale parameter $\hat{\alpha}$ versus the relative bias in the mean excess over the 99th percentile $Q_{0.99}$. The *numbers* correspond to the five regions, the *squares* to the basin-averages and the *black lines* to the least-squares fit to the regional biases of all RCM simulations

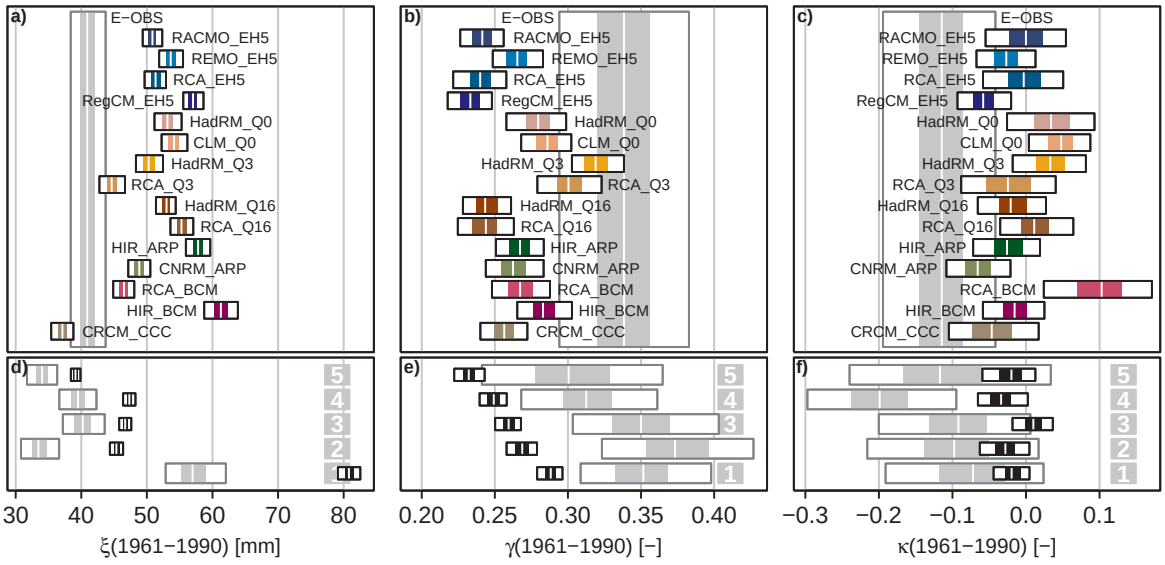

Fig. 6 As Fig. 4 but for the 5-day winter (DJF) precipitation extremes

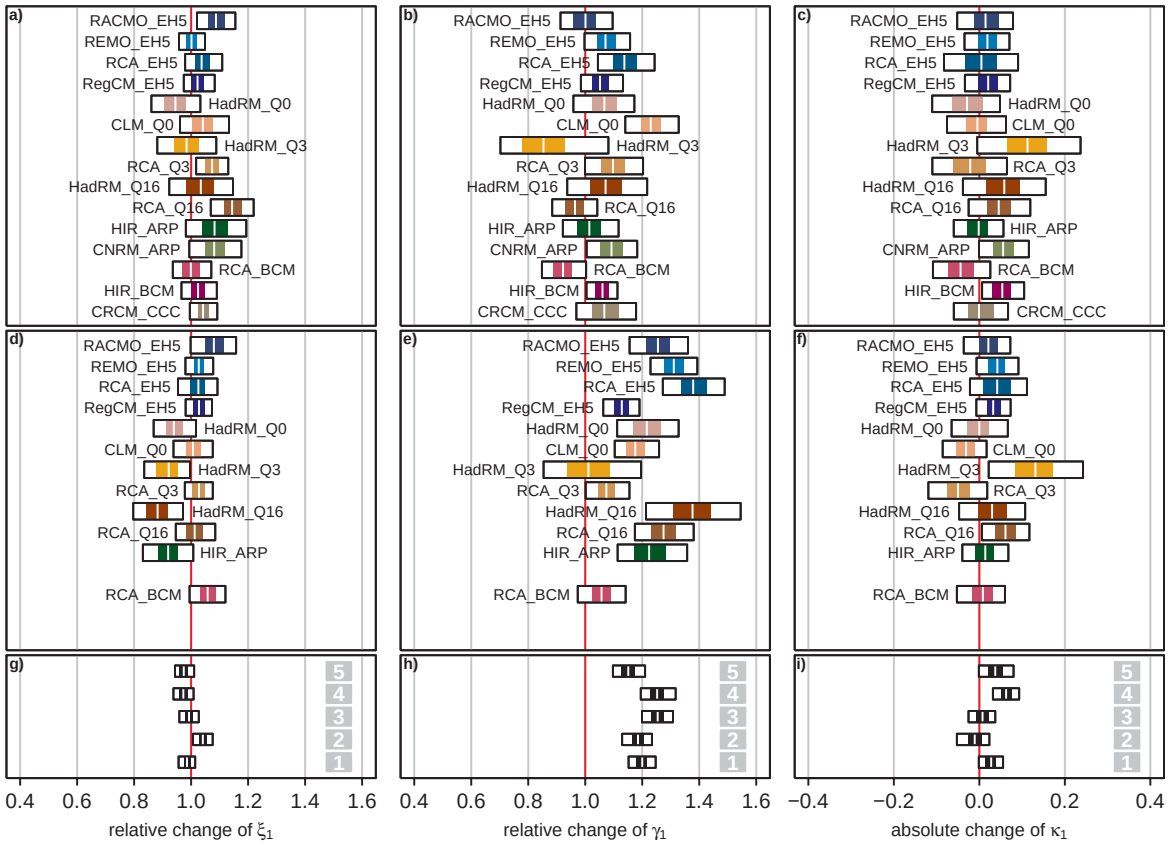

Fig. 7 Relative (for ξ and γ) or absolute (for κ) changes of the GEV parameters for the 1-day summer (JJA) precipitation extremes: **a–c** the basin-average changes between the periods 1961–1990 and 2031–2050, **d–f** the basin-average changes between the periods 1961–1990 and 2070–2099, **g–i** the average changes for each of the five regions of the Rhine basin between the periods 1961–1990 and 2070–2099 for the ensemble of RCM simulations longer than 100 years (*black boxes*). The boxplots are based on 500 bootstrap samples. The 5th, 25th, 50th, 75th and 95th percentiles of these bootstrap samples are indicated

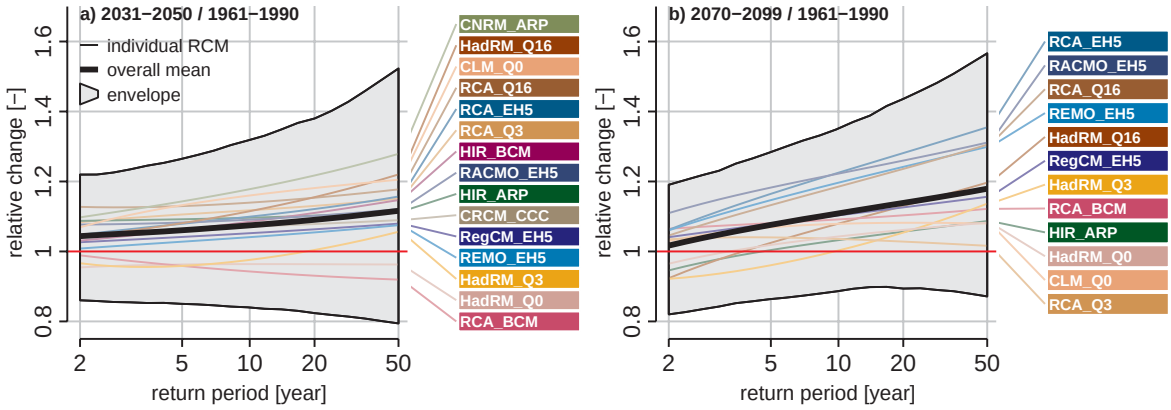

Fig. 8 Basin-average relative changes in quantiles for the 1-day summer (JJA) precipitation extremes between the periods **a** 1961–1990 and 2031–2050, and **b** 1961–1990 and 2070–2099. The *thin lines* correspond to the basin-average for the individual RCMs, the *thick line* to the overall mean. The (piecewise linear) *envelopes* indicate the 5th percentile of the minimum and the 95th percentile of the maximum relative basin average change in 500 bootstrap samples

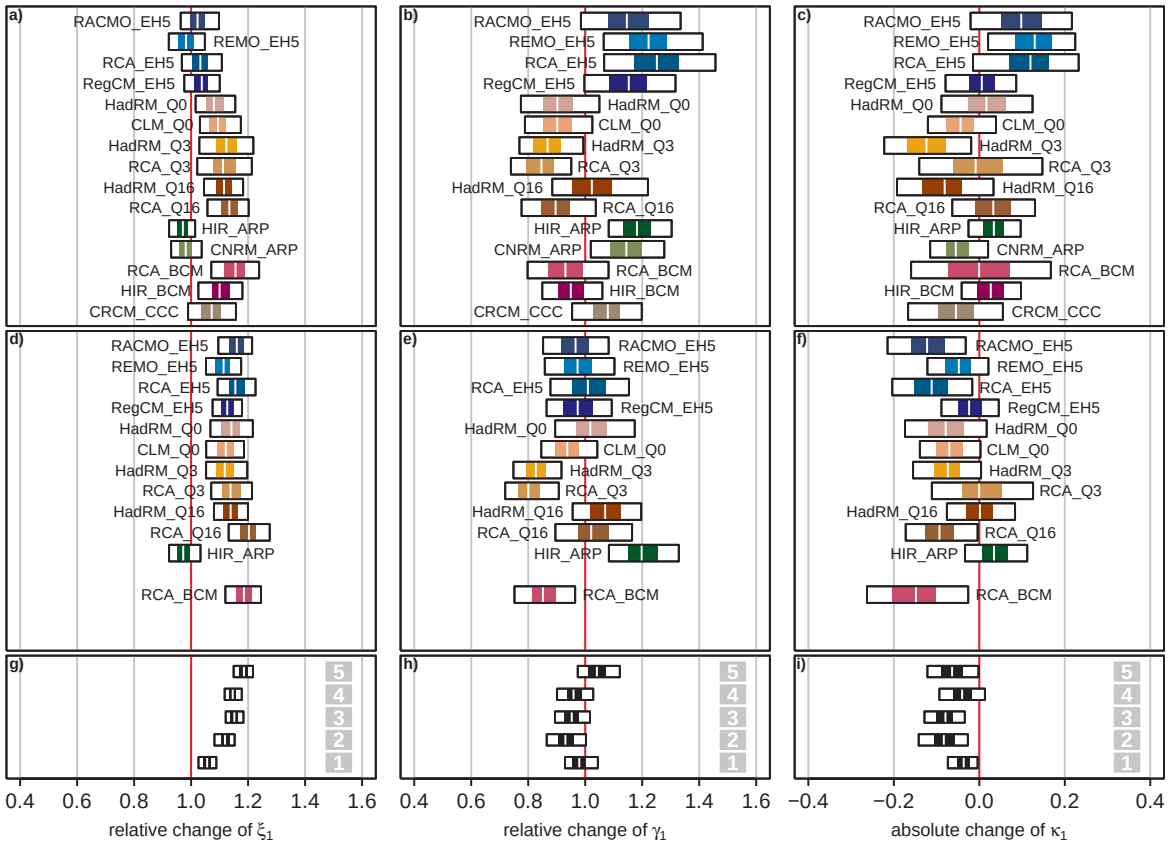

Fig. 9 As Fig. 7 but for the 5-day winter (DJF) precipitation extremes

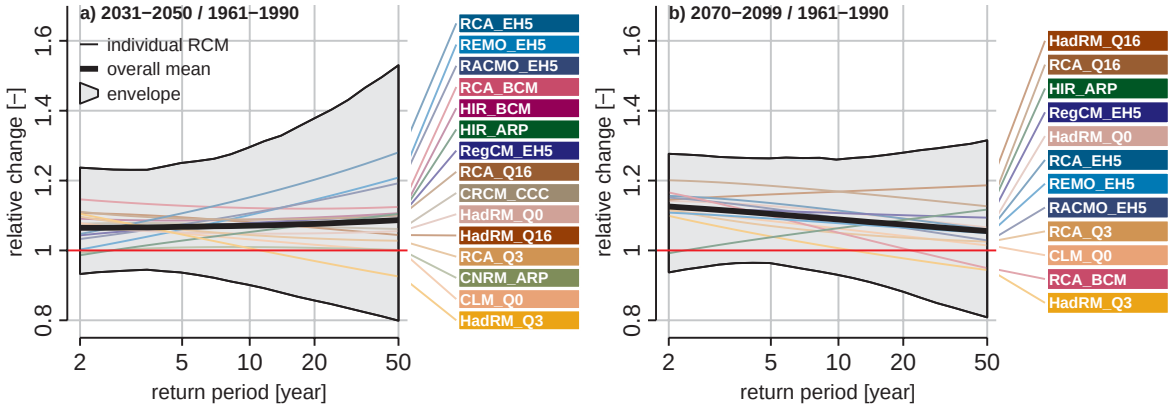

Fig. 10 As Fig. 8 but for the 5-day winter (DJF) precipitation extremes

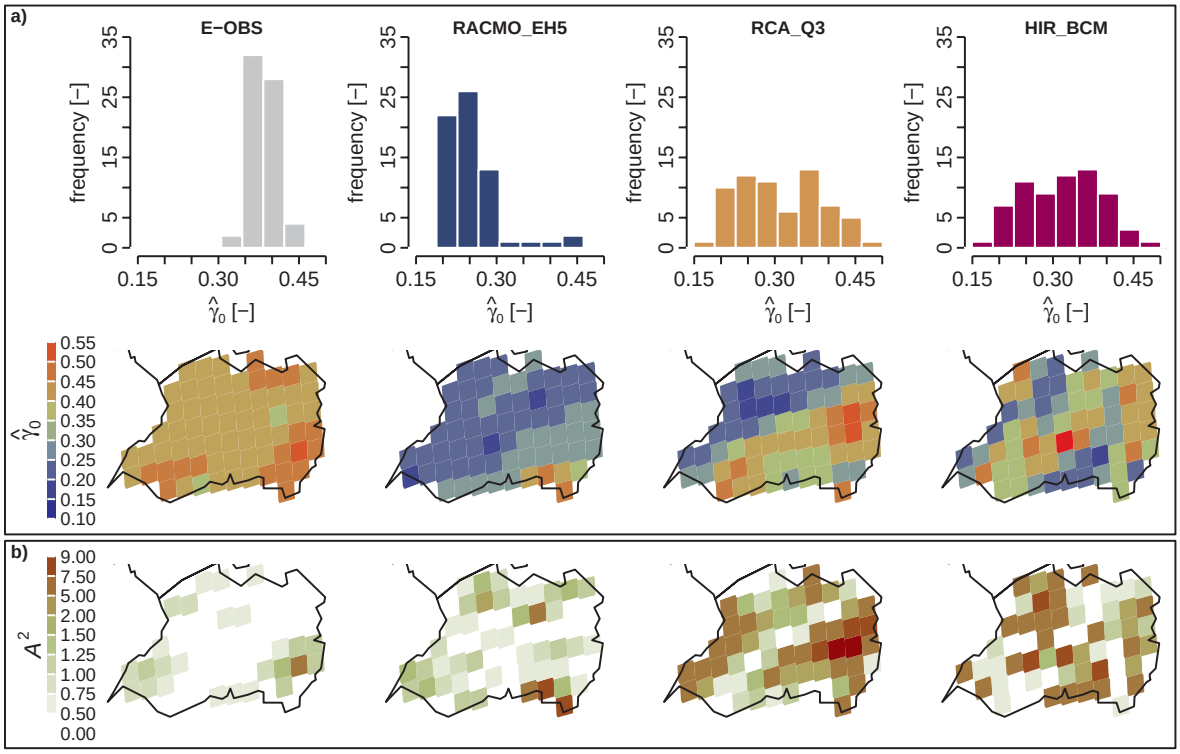

Fig. 11 a Histograms and spatial distribution of the estimated dispersion coefficient for the 5-day winter precipitation extremes in region 1 based on the fit of the stationary model to the precipitation maxima of each grid box for the period 1961–1990. **b** The spatial distribution of the A^2 statistic for the non-stationary index-flood model

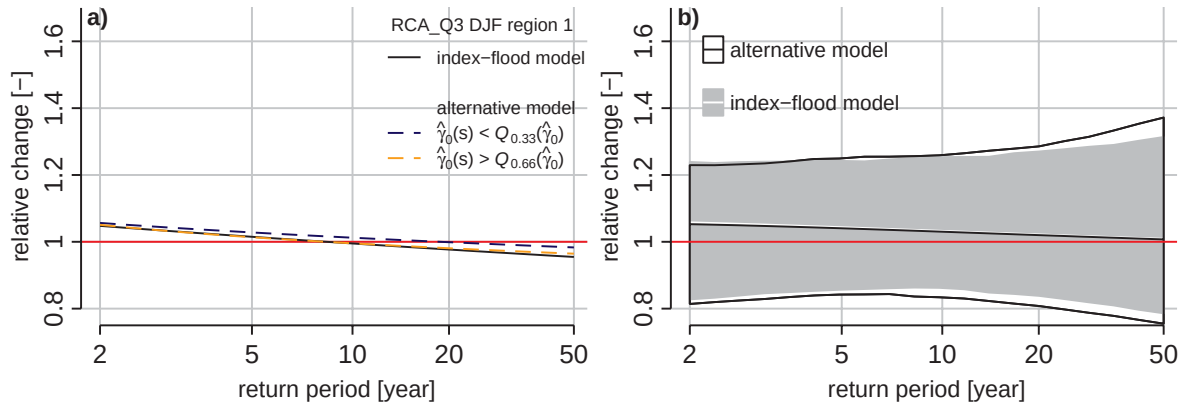

Fig. 12 Relative changes in the quantiles of the 5-day winter precipitation extremes in region 1 between the periods 1961–1990 and 2070–2099: **a** for the RCA_Q3 simulation as obtained from the non-stationary index-flood model (*black line*) and the alternative non-stationary GEV model for the grid boxes with $\hat{\gamma}_0(s) < Q_{0.33}(\hat{\gamma}_0)$ (*dashed blue line*) and those with $\hat{\gamma}_0(s) > Q_{0.66}(\hat{\gamma}_0)$ (*dashed orange line*), and **b for** the ensemble mean of the regional average of these changes as obtained from the non-stationary index-flood (*white line*) and the alternative non-stationary GEV (*black line*) model. The *gray area* and the *area between the black envelopes* indicate the interval between the 5th percentile of the minimum and the 95th percentile of the maximum relative regional average changes in 500 bootstrap samples for the non-stationary index-flood model and the alternative non-stationary GEV model, respectively

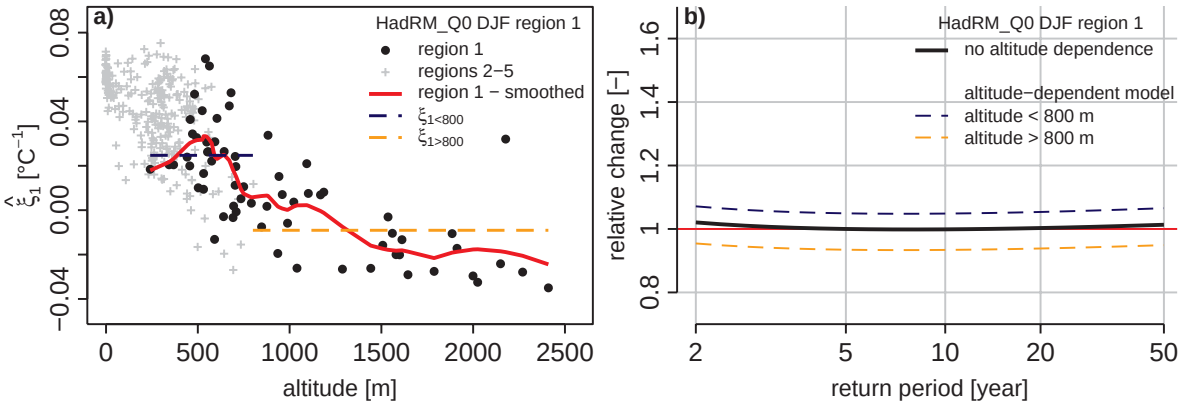

Fig. 13 a Estimates of ξ_1 for the 5-day winter precipitation maxima in region 1 (*black dots*) and regions 2–5 (*gray pluses*) for the HadRM_Q0 simulation. The values for the grid boxes in region 1 are smoothed by locally weighted regression "loess" (*red line*), the *dashed horizontal lines* correspond to the estimated values of $\xi_{1<800}$ and $\xi_{1>800}$ from the non-stationary index-flood model that allows for an altitude dependence of the trend in the location parameter. **b** The corresponding relative change in the quantiles from the

altitude dependent model (*dashed blue* and *orange line*, respectively) and the model with constant trend ξ_1 in the location parameter (*black line*)